JCTC Journal of Chemical Theory and Computation

Article

pubs.acs.org/JCTC

Accurate Prediction of Hyperfine Coupling Constants in Muoniated and Hydrogenated Ethyl Radicals: *Ab Initio* Path Integral Simulation Study with Density Functional Theory Method

Kenta Yamada,[†,§] Yukio Kawashima,[‡] and Masanori Tachikawa[†,*]

[†]Quantum Chemistry Division, Graduate School of Science, Graduate School of Nanobioscience, Yokohama City University, Yokohama 236-0027, Japan

[‡]RIKEN Advanced Institute for Computational Science, Minatojima-minami-machi 7-1-26, Chuo-ku, Kobe 650-0047, Japan

Supporting Information

ABSTRACT: We performed *ab initio* path integral molecular dynamics (PIMD) simulations with a density functional theory (DFT) method to accurately predict hyperfine coupling constants (HFCCs) in the ethyl radical ($C_\beta H_3-C_\alpha H_2$) and its Mu-substituted (muoniated) compound ($C_\beta H_2Mu-C_\alpha H_2$). The substitution of a Mu atom, an ultralight isotope of the H atom, with larger nuclear quantum effect is expected to strongly affect the nature of the ethyl radical. The static conventional DFT calculations of $C_\beta H_3-C_\alpha H_2$ find that the elongation of one C_β–H bond causes a change in the shape of potential energy curve along the rotational angle via the imbalance of attractive and repulsive interactions between the methyl and methylene groups. Investigation of the methyl-group behavior including the nuclear quantum and thermal effects shows that an unbalanced $C_\beta H_2Mu$ group with the elongated C_β–Mu bond rotates around the $C_\beta-C_\alpha$ bond in a muoniated ethyl radical, quite differently from the $C_\beta H_3$ group with the three equivalent C_β–H bonds in the ethyl radical. These rotations couple with other molecular motions such as the methylene-group rocking motion (inversion), leading to difficulties in reproducing the corresponding barrier heights. Our PIMD simulations successfully predict the barrier heights to be close to the experimental values and provide a significant improvement in muon and proton HFCCs given by the static conventional DFT method. Further investigation reveals that the C_β–Mu/H stretching motion, methyl-group rotation, methylene-group rocking motion, and HFCC values deeply intertwine with each other. Because these motions are different between the radicals, a proper description of the structural fluctuations reflecting the nuclear quantum and thermal effects is vital to evaluate HFCC values in theory to be comparable to the experimental ones. Accordingly, a fundamental difference in HFCC between the radicals arises from their intrinsic molecular motions at a finite temperature, in particular the methyl-group behavior.

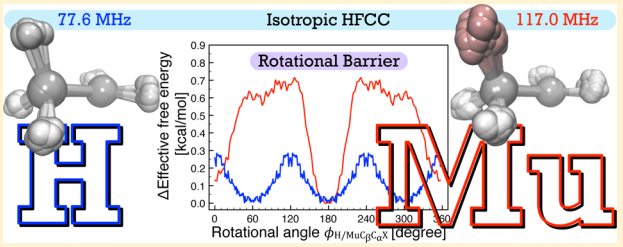

1. INTRODUCTION

Muon and muonimum chemistry has been addressed by experimental chemists, and a considerable amount of knowledge has been accumulated for over 30 years.[1−7] The negative muon (μ^-) and its antiparticle, positive muon (μ^+), are used to mimic the basis properties of an electron (e^-) and a proton (H^+), respectively. The muonium (Mu) atom, one of the exotic atoms, is a bound state of μ^+ and capturing an e^- ($Mu \equiv \mu^+e^-$); this atom, where H^+ is replaced by μ^+ with one-ninth of the mass of H^+, can indeed be regarded as an ultralight isotope of a H atom, i.e., Mu = $^{0.113}$H. It is noteworthy that while μ^+ is equal in spin and charge to H^+, μ^+ has a smaller mass, larger magnetic moment, and much shorter mean lifetime compared to H^+. With these unique features, various practical applications are being actively developed. For instance, the muon spin resonance/rotation/relaxation (μSR or MuSR), which is the collection of methods exploiting the muon spin, has been developed to observe structural and dynamical processes in the bulk of a material on a microscopic scale.[8−10] By using μ^- as a heavier electron, some properties of atoms and molecules such as the kinetic isotope effect (KIE) have been measured with heavy isotopes of the H atom, such as a bound state of He^{2+}, e^-, and μ^- ($He^{2+}e^-\mu^-$ or $^{4.113}$H).[11,12] Muon-catalyzed nuclear fusion for energy production has been studied with light nuclei pairs such as DT and DD.[13−15] Further, quantum reaction dynamics and "vibrational bonding" of heavy−light−heavy (H−L−H) systems with a Mu atom instead of with a H atom, such as Br−Mu−Br, Cl−Mu−Cl, and so on, have been debated.[16−18]

The μSR/MuSR plays a central role in muonium chemistry because of its extensive applications in condensed matter physics and chemistry.[19−27] Similarly to electron paramagnetic resonance (EPR), the hyperfine coupling constant (HFCC) in μSR/MuSR is a good index indicating the magnitude of magnetic interaction between electron and muon spins. The HFCC of μ^+ is determined by an electron spin density at μ^+, which is related to geometric structure, through direct and

Received: January 12, 2014
Published: April 8, 2014

indirect interaction between μ^+ and an unpaired electron. It is well-known that HFCC can be divided into an isotropic component (Fermi contact term) and an anisotropic component, arising from interactions between μ^+ and the spin density at μ^+ and between μ^+ and the densities at other nuclei, respectively. For μSR/MuSR experiments, a theoretical approach can make a substantial contribution to the structural characterization of muoniated radicals with short lifetimes. On the basis of the definition of isotropic HFCC of a normal nucleus,[28] μ^+ HFCC can be defined as (in Gauss)

$$A_\mu = \frac{8\pi g_e g_\mu \beta_B \beta_\mu}{3n} \sum_{r,s} \langle \chi_r | 2\hat{S}_{z1} \delta(r_{1\mu} - R_\mu) | \chi_s \rangle D_{rs} \quad (1)$$

where $\hat{S}_{z1}$ is the z component of the electron spin angular momentum operator, $\delta(r)$ is the delta function, n and D_{rs} are the number of unpaired electrons and the density matrix, respectively, g_e and g_μ are the electron and muon g factors, respectively, β_B and β_μ are the Bohr and "muon" magnetons, respectively, $r_{1\mu}$ and R_μ denote the position of the electron with respect to the muon and that of the muon, respectively, and $\{\chi_r\}$ represents atomic basis functions. Note that the product of the muon g factor and magneton is larger by about 3.183 than that of the proton g factor and nuclear magneton, and this constant is equal to the ratio of the positive muon magnetic moment to the proton magnetic moment.

Isotropic HFCC (hereafter called HFCC) is very sensitive to particularly both the quality of the one-particle basis functions attributable to the delta function in eq 1 and the level of theory to the reliable description of electronic structure and spin polarization; it is one of the properties that is difficult to calculate accurately.[29−31] For accurate prediction of HFCC, computational approaches have to be improved in the following two aspects: basis set and method.[32−37] In recent years, density functional theory (DFT) methods, which can in principle give a correct nuclear-electron cusp,[38,39] have been widely used to calculate HFCC values with reasonable reliability.[35−37,40−43] As well as hydrogenated (unsubstituted) free radicals, muoniated ones are widely studied to interpret and rationalize experimental results.[44−46] In these studies, μ^+ HFCCs cannot be comparable to experimental results, which can exhibit, at 300 K, a 30−40% increase in HFCC compared to hydrogenated radicals because of a significant isotope effect originating from small mass of μ^+.[47] This is because static conventional DFT methods that treat nuclei as point charges cannot represent nuclear quantum effect. To briefly describe a change induced by this effect, a scale factor for a bond length optimized by static conventional methods is used in several papers.[48,49] However, there is no guarantee that the effect due to Mu substitution has an influence only on bond lengths.

Many previous studies have demonstrated that the quantum behavior of the proton has a powerful influence on properties of systems, such as molecular geometries and reaction pathways.[50,51] Among them we have shown that in various molecular systems the quantum effect of proton makes a distinction between *equilibrium* structure by static conventional methods and *averaged* structure over geometric configurations reflecting nuclear quantum and thermal effects;[52,53] these configurations have been obtained from the path integral molecular dynamics method with *ab initio* theory (*ab initio* PIMD approach), which is a promising approach to describe the nature of molecules.[54,55] Because a muon with a smaller mass (0.113 amu) exhibits a larger quantum effect than a proton (1.008 amu), it is indispensable to consider this effect to understand the nature of a muoniated system. The *ab initio* PIMD approach is capable of introducing, under the Born−Oppenheimer approximation, nuclear quantum and thermal effects to conventional calculations. Previous studies have shown that the Mu atom is sufficiently heavy compared to an electron,[56,57] and hence the PIMD approach is applicable to a muoniated system to provide an appropriate description of quantum behavior, which has been proven for protons.

The ethyl radical ($C_\beta H_3-C_\alpha H_2$) is one of the simplest carbon-centered free radicals, and it has been extensively applied to the study of its electronic and magnetic properties, such as HFCC values with vibrational averaging correction, the internal rotation barrier of the methyl group, and the variation in H^+ HFCC values with this rotation.[58−67] These values, especially methyl H^+ HFCCs, are affected by the rotation via electron spin densities at the corresponding nuclei. This density is dependent on structural parameters, such as the C_β−H bond lengths, and on the competition between through-space (direct) and through-bond (indirect) interactions involving a radical orbital on the C_α atom containing an unpaired electron. Further, the methyl-group rotation in the ethyl radical is correlated with the $C_\beta-C_\alpha H_2$ (methylene-group) pyramidalization (rocking motion), following experimental and theoretical studies.[64,65] Accordingly, overall molecular motion has to be considered to reproduce experimental HFCC values.

The substitution of one of the methyl H atoms in the ethyl radical with a Mu atom gives a muoniated ethyl radical, $C_\beta H_2Mu-C_\alpha H_2$, on which we focus in this paper. Several μSR/MuSR experiments in the gas phase[68−70] revealed the barrier height of the $C_\beta H_2Mu$-group rotation around the $C_\beta-C_\alpha$ bond to be different from the $C_\beta H_3$-group rotation in the ethyl radical. This suggests that the Mu atom causes a large change in the nature of the original system, such as molecular structure and properties. Concerning this isotope effect, theoretical studies have been reported.[57,71−74] Among them, PI Monte Carlo (PIMC) simulations with the tight-binding method showed the temperature dependence (25−1000 K) of the nuclear quantum effect on probability density distributions of the nuclei and distribution functions of the HFCCs in the muoniated ethyl radical. Although they confirmed that the internal rotation in the muoniated ethyl radical differs markedly from that in the unsubstituted one, the rotational barrier height was not present from an energetic viewpoint, and μ^+ HFCC was overestimated by more than 50 MHz. We reported that the $C_\beta H_2Mu$-group rotation correlates with the C_β−Mu bond stretching and methylene-group rocking motions of the muoniated ethyl radical using the PIMD approach with the semiempirical PM6 method.[75] Meanwhile, because of the limitation of the semiempirical theory, the simulation failed to predict μ^+ and H^+ HFCCs in the muoniated radical quantitatively, though it improved their absolute relationship. This means that more reliable interatomic potential than semiemprical PM6 potential needs to be employed to predict the HFCC values. Furthermore, one of the authors reported that with PIMD simulation an accurate reaction barrier provides the correct description of proton transfer, where the nuclear quantum effect plays an important role.[76] Therefore, it can be stated that quantitative HFCC values in muoniated and hydrogenated ethyl radicals result from the nuclear quantum and thermal effects as well as high-level electronic structure calculations, which can accurately describe the reaction barrier.

In this paper, thus, we perform *ab initio* PIMD simulations with a DFT method to show that this simulation, based on reliable electronic structure, accurately reproduces the HFCC values in the methyl groups of the radicals. The intrinsic methyl-group rotation, intimately linked to other molecular motions, is important for accurate HFCC values. To represent these motions, the simulations are done without any constraints on atoms or degrees of freedom. This paper is organized as follows. The next section provides computational details about the PI scheme and our *ab initio* PIMD approach in addition to the definition of structural parameters in a muoniated ethyl radical (hereafter denoted as Mu radical) and hydrogenated ethyl radical (hereafter denoted as H radical). In the Results and Discussion section, after we start our discussion of the validity of the DFT method employed here, the geometric structure is examined using static conventional calculations. Then compared to these results, structural fluctuations and predicted HFCCs in the electronic ground states of the two radicals, obtained from the PIMD simulations, are discussed. Finally, concluding remarks are given.

2. COMPUTATIONAL DETAILS

To quantitatively investigate the difference in structural characteristics between Mu and H ethyl radicals and estimate their hyperfine coupling constants (HFCCs), we perform the following three simulations: (1) the conventional static DFT calculation, (2) conventional *on-the-fly ab initio* molecular dynamics (MD) simulation with the DFT method, and (3) *on-the-fly ab initio* path integral molecular dynamics (PIMD) simulations with the DFT method. The first calculation assuming nuclei as conventional "classical" point charges provides the optimized structure without nuclear quantum or thermal effects, called equilibrium (EQ) structure. The second simulation is that thermal effect is incorporated into the first calculation, and the third simulation can provide results taking not only thermal but also nuclear quantum effect into account. The former can be regarded as a nuclear *classical* simulation and the latter a nuclear *quantum* simulation.

The standard imaginary-time PIMD simulations in normal mode coordinates[77,78] were carried out to achieve thermal equilibrium of the target system including nuclear quantum effect directly. According to the PI scheme, the partition function for the canonical ensemble in the quantum statistics of an M particle system is described as an $M \times P$ classical particle system using an effective potential:

$$V_{\mathrm{eff}} = \sum_{s=1}^{P}\sum_{i=1}^{M}\frac{m_i P}{2\beta^2\hbar^2}(\mathbf{R}_i^{(s+1)} - \mathbf{R}_i^{(s)})^2 + \frac{1}{P}\sum_{s=1}^{P} V(\mathbf{R}_1^{(s)}, \mathbf{R}_2^{(s)}, ..., \mathbf{R}_M^{(s)}) \quad (2)$$

with the cyclic condition, $\mathbf{R}_i^{(P+1)} = \mathbf{R}_i^{(1)}$. In this equation, $\beta = 1/k_B T$ where k_B and T are the Boltzmann constant and temperature, respectively; P and $\hbar$ are the number of the imaginary time slice and reduced Plank constant, respectively; and m_i and $\mathbf{R}_i^{(s)}$ are the mass of ith nucleus and the coordinate of the sth slice of the ith nucleus, respectively. In this paper, we used the Born−Oppenheimer potential energy values (V) and their first derivatives with respect to the nuclear positions ($\{\mathbf{R}_i^{(s)}\}$) generated *on-the-fly* by the DFT method. P is also known as the Trotter number or number of beads, which is varied for the system, and the m_i's of H and Mu atoms are 1.008 and 0.113 amu, respectively.

In this study, to effectively control the system temperature, the massive Nosé−Hoover chain thermostat with chain length parameter 4 was exploited. The equation of motion was integrated using the velocity-Verlet time integrator under multiple time step technique.[79] The nuclear quantum simulations were conducted at 300 K with (P, imaginary-time step) = (64, 40 as) and (16, 0.1 fs) for the Mu and H ethyl radicals, respectively. Note that the appropriate number of imaginary time slices (P = 64) to represent the "cloud" of μ^+ was determined by the convergence of the C_β−Mu bond length with respect to P.[75] In each of our PIMD simulations, the production run was carried out for 90 000 steps after a thermal equilibration of 10 000 steps. The nuclear classical simulation consists of data collection of 650 000 steps preceded by a thermal equilibration of 100 000 steps under the condition of the same temperature and a 0.1 fs time step. The *ab initio* PIMD simulations were performed with our PIMD code, which is in conjunction with the Gaussian 09 program package.[80]

Figure 1 gives a schematic representation of the H radical, constituted of methyl and methylene groups, where the H_1 atom is substituted with the Mu atom in the Mu radical. One fictitious position of X shown as the purple ball in Figure 1 is used to monitor the methyl-group rotation. For this purpose, $\mathbf{R}_A$ is employed to describe the coordinate of the A atom and $\mathbf{R}_{AB}$ denotes $\mathbf{R}_B - \mathbf{R}_A$. The dihedral angle Mu/$H_1$−$C_\alpha$−$C_\beta$−X on which we focused in this paper indicates the angle between the two planes of the {Mu/H_1, C_β, C_α} atoms and {C_β, C_α, X} atoms. To observe the rotation together with an inversion of the methylene group, belonging to the C_β−$C_\alpha H_2$ rocking motion, a rotational angle is defined with the position X determined via a temporary position vector $\tilde{\mathbf{R}}_{C_\alpha X}$:

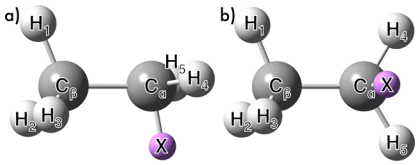

Figure 1. Side view of representative structures of the (hydrogenated) ethyl radical in (a) eclipsed and (b) staggered conformations ($\phi_{H_1C_\beta C_\alpha X}$ = 180° and $\phi_{H_1C_\beta C_\alpha X}$ = 90°/270°, respectively). The atom labeling scheme is given together with the position X, which is introduced to define rotational angles. The H_1 atom in this figure was replaced with a Mu atom for the muoniated ethyl radical.

$$\mathbf{R}_{C_\alpha X} = \begin{cases} \tilde{\mathbf{R}}_{C_\alpha X} & \text{for } \mathbf{R}_{C_\alpha C_\beta}\cdot\tilde{\mathbf{R}}_{C_\alpha X} \le 0 \\ -\tilde{\mathbf{R}}_{C_\alpha X} & \text{otherwise} \end{cases} \quad (3)$$

where

$$\tilde{\mathbf{R}}_{C_\alpha X} = \mathbf{R}_{C_\alpha H_5} \times \mathbf{R}_{C_\alpha H_4} \quad (4)$$

The rotational angle with X thus obtained is represented as $\phi_{MuC_\beta C_\alpha X}$ for the Mu radical ($\phi_{H_1C_\beta C_\alpha X}$ for H radical). Also, to track the rocking motion, the rocking angle is defined as

$$\theta_{\mathrm{rock}} = 180 - \arccos\left(\frac{\mathbf{R}_{C_\alpha C_\beta}}{|\mathbf{R}_{C_\alpha C_\beta}|}\cdot\frac{1}{\sqrt{2}}\left(\frac{\mathbf{R}_{C_\alpha H_4}}{|\mathbf{R}_{C_\alpha H_4}|} + \frac{\mathbf{R}_{C_\alpha H_5}}{|\mathbf{R}_{C_\alpha H_5}|}\right)\right) \quad (5)$$

dx.doi.org/10.1021/ct500027z | J. Chem. Theory Comput. 2014, 10, 2005−2015

While this angle is always positive, positive and negative values of the angle are defined by eq 6 to discuss the inversion.

$$\tilde{\theta}_{\mathrm{rock}} = \begin{cases} \theta_{\mathrm{rock}} & \text{for } \mathbf{R}_{C_\alpha C_\beta} \cdot \tilde{\mathbf{R}}_{C_\alpha X} \leq 0 \\ -\theta_{\mathrm{rock}} & \text{otherwise} \end{cases} \quad (6)$$

3. RESULTS AND DISCUSSION

3.1. Static Calculation: Choice of the Density Functional Theory (DFT) Method. Before starting simulations, the reliability of the method for potential energy calculations of the Mu and H radicals needs to be assessed. The potential energy difference between eclipsed ($\phi_{H_1C_\beta C_\alpha X}$ = 180°) and staggered ($\phi_{H_1C_\beta C_\alpha X}$ = 90°/270°) ethyl radicals, as seen in Figure 1, serves as a suitable index for assessment. The energy difference using the CCSD(T)/aug-cc-pVTZ//MP2/aug-cc-pVTZ method[81−83] was regarded as the most reliable value, and thus chosen as a reference. Table 1 lists the differences calculated at various levels of theory, i.e., semiempirical PM6, Hartree−Fock (HF), and DFT methods,[84−90] with the structures optimized using each method and the MP2 structure. Note that in this study, we employed the 6-31G(d,p) basis set[91,92] based on the balance between computational speed and useful accuracy. Table 1 shows that the DFT results are closer to the reference than the HF and PM6 ones, and especially the O3LYP/6-31G(d,p) result coincides (see also Figure S7). Accordingly, we decided to use the O3LYP/6-31G(d,p) method in our nuclear classical and quantum simulations.

3.2. Static Calculation: Potential Energy Curves Along the Rotational Angle. To gain insight into the methyl-group rotation, potential energy curves (PECs) of the H radical were examined using the static conventional O3LYP/6-31G(d,p) method. This examination was done under the condition that the methyl group rotates around the C_β−C_α bond axis with all structure parameters except the rotational angle $\phi_{H_1C_\beta C_\alpha X}$ fixed to those obtained from the PIMD simulation for the H radicals (see below and Figure S8). Figure 2 depicts variations in PECs with respect to $\phi_{H_1C_\beta C_\alpha X}$ for several bond lengths ($R_{C_\beta H_1}$): (1) $R_{C_\beta H_1}$ equal to other methyl C_β−H bond lengths of 1.12 Å, (2) $R_{C_\beta H_1}$ = 1.06 Å shorter than other methyl C_β−H ones, (3) $R_{C_\beta H_1}$ = 1.18 Å longer than other methyl C_β−H ones, and (4) $R_{C_\beta H_1}$ = 1.24 Å longer than the case of 3. Elongated $R_{C_\beta H_1}$ in the cases of 3 and 4 provides a simple model for the PEC of the Mu radical.

Figure 2 gives the following findings: (1) When $R_{C_\beta H_1}$ is equal to $R_{C_\beta H_2}$ and $R_{C_\beta H_3}$, three minima (at $\phi_{H_1C_\beta C_\alpha X}$ = 60°, 180°, and 300°) and barriers (at $\phi_{H_1C_\beta C_\alpha X}$ = 0°, 120°, and 240°) are equivalent, respectively. (2) When $R_{C_\beta H_1}$ is shorter than $R_{C_\beta H_2}$ and $R_{C_\beta H_3}$, the methyl H_1 atom has more repulsive interaction with the methylene group. The minimum at $\phi_{H_1C_\beta C_\alpha X}$ = 180° is less stable than the other two minima at $\phi_{H_1C_\beta C_\alpha X}$ = 65° and 295°, and the barrier at $\phi_{H_1C_\beta C_\alpha X}$ = 0° is higher than the other two barriers. This indicates that at these angles the H_1 atom interacts more strongly with the methylene group. (3) When $R_{C_\beta H_1}$ is longer than $R_{C_\beta H_2}$ and $R_{C_\beta H_3}$, the methyl H_1 atom has a less repulsive interaction with the methylene group. In contrast to case 1, the minimum at $\phi_{H_1C_\beta C_\alpha X}$ = 180° is more stable than the other two minima, and the barrier at $\phi_{H_1C_\beta C_\alpha X}$ = 0° is lower

Table 1. Energy Differences between Eclipsed and Staggered Conformations[a,b] Obtained Using DFT, HF, and PM6 Methods [in kcal/mol]

	DFT/6-31G(d,p)									
	O3LYP	B3LYP	B3PW91	B3P86	ωB97X	M06	HF/6-31G(d,p)	PM6	reference[c]
ΔE_1 ($\Delta\Delta E_1$)	−0.085 (0.001)	−0.083 (0.003)	−0.079 (0.007)	−0.077 (0.009)	−0.070 (0.016)	−0.094 (−0.008)	−0.165 (−0.078)	−0.005 (0.081)	−0.086
ΔE_2 ($\Delta\Delta E_2$)	−0.084 (0.002)	−0.082 (0.004)	−0.078 (0.008)	−0.075 (0.011)	−0.070 (0.017)	−0.093 (−0.006)	−0.146 (−0.060)	0.269 (0.355)	−0.086

[a] ΔE = E(eclipsed conformation) − E(staggered conformation). [b] ΔE_1 and ΔE_2 are the energy differences (ΔE) with the structure optimized using the same method as the electronic structure calculation and those with the MP2-optimized structure, respectively. [c] The CCSD(T)/aug-cc-pVTZ//MP2/aug-cc-pVTZ result is used.

dx.doi.org/10.1021/ct500027z | J. Chem. Theory Comput. 2014, 10, 2005−2015

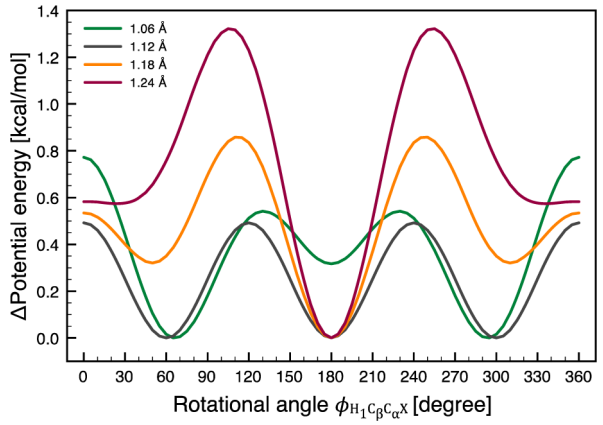

Figure 2. Potential energy curves along the rotational angle ($\phi_{H_1C_\beta C_\alpha X}$) for several C_β–H_1 bond lengths under the condition that other structural parameters are fixed to the PIMD structure of the H radical.

than the other two barriers. (4) When $R_{C_\beta H_1}$ is much longer than $R_{C_\beta H_2}$ and $R_{C_\beta H_3}$, it is likely that the two minima disappear and the barrier found at $\phi_{H_1C_\beta C_\alpha X} = 0°$ becomes a local minimum; in other words, this suggests that PEC with a more elongated $R_{C_\beta H_1}$ shows one global minimum, one local minimum, and two barriers. As $R_{C_\beta H_1}$ becomes larger, all rotational angles giving minima and barriers except at 0° and 180° are shifted away from 180°. The elongation of one C_β–H bond induces the change in the balance of interactions (hyperconjugation and repulsion) between the methyl and methylene groups, as found in the natural bond orbital (NBO) analysis with second-order perturbation theory[93,94] (see text and Figure S1 in the Supporting Information). Therefore, the C_β–H bond stretching motion has a significant influence on the determination of PEC and its closely related *actual* methyl-group rotation, being coupled with other molecular motions.

3.3. Quantum Simulation: Nuclear Quantum and Thermal Effects on Geometric Structure. Let us investigate geometric configurations from the PIMD simulations by comparison of bond-length and rotational distributions with those from other simulations and between the Mu and H radicals. Here, Table 2 gives all bond lengths of the Mu and H radicals obtained from nuclear quantum simulations together with those from the static conventional calculation and nuclear classical simulation. In the two simulation results, the bond lengths, $R_{C_\beta Mu}$, $R_{C_\beta C_\alpha}$, $R_{C_\beta H}$, and $R_{C_\alpha H}$, are the average values over the sampling runs; $R_{C_\beta H}$ and $R_{C_\alpha H}$ are further averaged over $R_{C_\beta H_2}$ and $R_{C_\beta H_3}$ and over $R_{C_\alpha H_4}$ and $R_{C_\alpha H_5}$, respectively. For the H radical, additionally, the average length of the three methyl C_β–H bonds is shown as $\bar{R}_{C_\beta H}$. The bond lengths from the nuclear quantum simulations become larger than those from other types of simulation. This is explained by the difference in anharmonicity of potentials along bonds that simulations can represent. Nuclear quantum simulation is a more sophisticated approach to represent the anharmonicity of the potential, and it can provide an actual potential with a thermal effect. In the quantum columns, $R_{C_\beta Mu}$ being much longer than $\bar{R}_{C_\beta H}$ demonstrates that as the mass of the atom bonded to the C_β atom is smaller, suggesting that the nuclear quantum effect of the corresponding nucleus is larger, the magnitude of the anharmonicity becomes larger.

Table 2. Structural Parameters in Muoniated and Hydrogenated Ethyl Radicals

		quantum		classical
structural parameters	conventional[a]	Mu radical	H radical	H radical
bond length [Å]				
$R_{C_\beta Mu}$	1.104	1.167		
$R_{C_\beta C_\alpha}$	1.486	1.492	1.495	1.493
$R_{C_\beta H}$[b]	1.096	1.120		
$\bar{R}_{C_\beta H}$[c]	1.099		1.119	1.102
$R_{C_\alpha H}$[d]	1.085	1.106	1.104	1.089
bond angle [degree]				
$\theta_{MuC_\beta C_\alpha}$	112.2	111.8		
$\theta_{HC_\beta C_\alpha}$[e]	111.9	112.0		
$\bar{\theta}_{HC_\beta C_\alpha}$[f]	112.0		111.9	111.9
$\theta_{C_\beta C_\alpha H}$[g]	120.9	102.2	120.4	120.4
rocking angle [degree]				
θ_{rock}	6.9	15.5	14.2	13.2

[a]The static conventional methods cannot distinguish HFCCs in the Mu radical from those in the H radical. [b]$R_{C_\beta H} = (R_{C_\beta H_2} + R_{C_\beta H_3})/2$. [c]$\bar{R}_{C_\beta H} = (R_{C_\beta H_1} + 2R_{C_\beta H})/3$. [d]$R_{C_\alpha H} = (R_{C_\alpha H_4} + R_{C_\alpha H_5})/2$. [e]$\theta_{HC_\beta C_\alpha} = (\theta_{H_2C_\beta C_\alpha} + \theta_{H_3C_\beta C_\alpha})/2$. [f]$\bar{\theta}_{HC_\beta C_\alpha} = (\theta_{H_1C_\beta C_\alpha} + 2\theta_{HC_\beta C_\alpha})/3$. [g]$\theta_{C_\beta C_\alpha H} = (\theta_{H_4C_\beta C_\alpha} + \theta_{H_5C_\beta C_\alpha})/2$.

It is noteworthy that the ratio of $R_{C_\beta Mu}$ between quantum simulation and conventional calculation is 1.057, corresponding to the scale factor for the bond length of the EQ structure. Previous studies[5,70,95] proposed that the C_β–Mu bond being longer than the C_β–H bond induces a "residual" isotope effect, which leads to a fundamental difference between μ^+ and H^+ HFCC values. It can be stated that an increase in the anharmonicity of the potential due to small mass, producing a large nuclear quantum effect, is responsible for the residual isotope effect via the difference in bond length if only this difference explains the increased HFCC value.

In addition to bond lengths, the rotational angles $\phi_{MuC_\beta C_\alpha X}$ and $\phi_{HC_\beta C_\alpha X}$ are dramatically different from those of the EQ structure. Figure 3 shows one-dimensional (1D) effective free

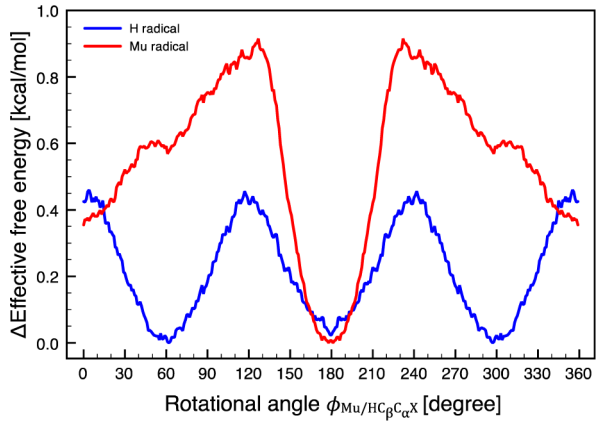

Figure 3. Effective free energy curves along the rotational angle ($\phi_{Mu/HC_\beta C_\alpha X}$) for muoniated and hydrogenated ethyl radicals from nuclear quantum simulations.

dx.doi.org/10.1021/ct500027z | J. Chem. Theory Comput. 2014, 10, 2005–2015

energy curves (FECs) along $\phi_{MuC_\beta C_\alpha X}$ and $\phi_{HC_\beta C_\alpha X}$. The 1D FEC is obtained as follows:

$$\Delta F(i) = -k_B T \ln W(i) + k_B T \ln W(i_{max}) \quad (7)$$

where $W(i)$ is the probability in the ith horizontal bin and i_{max} gives the largest of $\{W(i)\}$. Note that the probability $W(i)$ on the rotational angle is adjusted as

$$W(i) = W(i) + W(I - 1 - i) \quad (8)$$

where I is the number of the horizontal bins, because the rotational angle has a symmetric property with respect to the plane composed of $\{C_\beta, C_\alpha, X\}$ atoms. In Figure 3, the three equivalent minima are found at $\phi_{HC_\beta C_\alpha X} = 60°$, 180°, and 300° for the H radical, while the local and global minima are at $\phi_{MuC_\beta C_\alpha X} = 0°$ and 180° for the Mu radical. The shape of the 1D FEC for the H radical is consistent with chemical intuition, whereas that of the Mu radical is not. This clearly suggests that the Mu atom with the expanding μ^+ cloud affects the structural fluctuations involving the rotational angle, i.e., the methyl-group rotation around the C_β–C_α bond axis. Comparison of the FECs in Figure 3 with the PECs in Figure 2 shows that the FEC of the Mu radical corresponds to the PEC for case 4 and that the FEC of the H radical is in accord with the PEC for case 1. Furthermore, considering $R_{C_\beta Mu}$ from the PIMD simulation (1.167 Å), configurations with the bond more elongated are considered to have a strong influence on the FEC.

The theoretical barrier heights in Figure 3 are 0.46 and 0.92 kcal/mol for the H and Mu radicals, respectively. The former is consistent with our intuition that the methyl group is free to rotate at 300 K. The latter height suggests that the rotation of the Mu-substituted methyl group is rather limited at 300 K (~0.6 kcal/mol). The infrequent rotation would occur due to the tunneling effect (tunneling rotation).[96,97] According to previous experimental studies,[64,98] the corresponding barrier heights are 0.05 and 0.7 kcal/mol for the H and Mu radicals, respectively. Note that the rotational barriers in Figure 3 do not necessarily reproduce the experimental results because the horizontal axis in this 1D curve, onto which the multidimensional free energy landscape (FEL) described by *limited* internal degrees of freedom is projected, is not corresponding to the *actual* rotational pathway. That is, no facile pathway for the pure methyl-group rotations exists.

To monitor changes in the methyl-group rotation with the bond stretching motion, the two-dimensional (2D) FELs as a function of $R_{C_\beta Mu}$ and $\phi_{MuC_\beta C_\alpha X}$ and of $\bar{R}_{C_\beta H}$ and $\phi_{HC_\beta C_\alpha X}$ are shown in Figure 4a and b, respectively. Here, the 2D FEL is generated by

$$\Delta F(i, j) = -k_B T \ln W(i, j) + k_B T \ln W(i_{max}, j_{max}) \quad (9)$$

where $W(i, j)$ is the probability in the intersection of the ith horizontal and jth vertical bins and a pair of i_{max} and j_{max} yields the largest of $\{W(i,j)\}$. Similarly to FEC in Figure 3, $W(i,j)$ involving the rotational angle as the vertical axis is given as

$$W(i, j) = W(i, j) + W(i, J - 1 - j) \quad (10)$$

where J is the number of the vertical bins. Figure 4 demonstrates the correlation of the rotation with the stretching motion in both the radicals. In the Mu radical, the horizontally extended region at $\phi_{MuC_\beta C_\alpha X} = 180°$ is viewed as the global minimum. On the other hand, in the H radical there are three similar minima with a circular region at $\phi_{HC_\beta C_\alpha X} = 60°$, 180°, and 300°. Mu-substitution induces a dramatic change in not only bond lengths and the rotational angle but also their relationship. Figure 4a reveals that the rotational barrier just outside the region of the global minimum ($\phi_{MuC_\beta C_\alpha X} \approx 125°$ and 235°) should be overcome with the bond length confined to the small range around the average length, and that as $\phi_{MuC_\beta C_\alpha X}$ approaches the local minimum, i.e., 0° (360°), the stability in the larger range increases again. It can be stated that the methyl C_β–Mu bond length is generally difficult to determine, even in the case of the H radical, unless other structural parameters such as the rotational angle are considered.

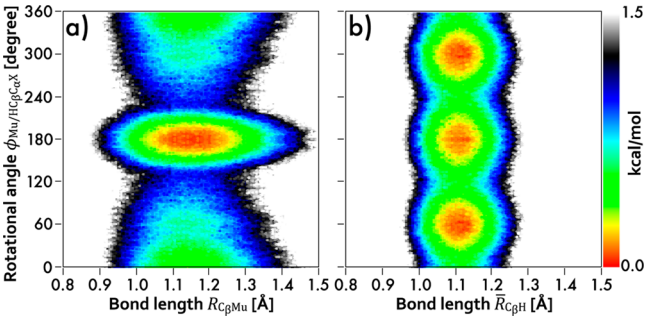

Figure 4. Free energy landscapes as a function (a) of the C_β–Mu bond length ($R_{C_\beta Mu}$) and rotational angle ($\phi_{MuC_\beta C_\alpha X}$) and (b) of the C_β–H bond length averaged over the three equivalent bonds ($\bar{R}_{C_\beta H}$) and rotational angle ($\phi_{HC_\beta C_\alpha X}$).

The influence of the methylene-group rocking motion, one of the other degrees of freedom, on the pathway is non-negligible because this motion is involved in the methyl-group rotation[63] through intragroup interactions described in subsection 3.2. To understand the relationship between the methylene-group rocking and methyl-group rotational distributions, 2D FELs as a function of $\tilde{\theta}_{rock}$ and $\phi_{MuC_\beta C_\alpha X}$ for the Mu radical and of $\tilde{\theta}_{rock}$ and $\phi_{HC_\beta C_\alpha X}$ for the H radical are depicted in Figure 5. To characterize the rocking distribution of the methylene group, the positive and negative rocking angles ($\tilde{\theta}_{rock}$) defined as eq 6 indicate those with the noninverted and inverted group, respectively, with reference to the EQ structure where the group is noninverted. Figure 5 shows that in both the radicals, the C_β atom and methylene group are rarely in the

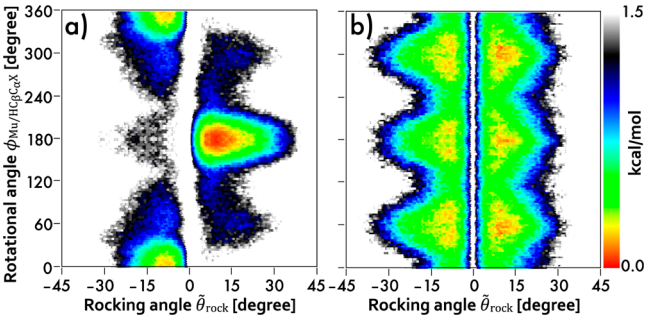

Figure 5. Free energy landscapes as a function (a) of the signed rocking angle ($\tilde{\theta}_{rock}$) and rotational angle ($\phi_{MuC_\beta C_\alpha X}$) and (b) of the signed rocking angle ($\tilde{\theta}_{rock}$) and rotational angle ($\phi_{HC_\beta C_\alpha X}$) for the Mu and H radicals, respectively. Positive and negative $\tilde{\theta}_{rock}$ serve as the rocking angles (θ_{rock}) of the uninverted and inverted methylene groups, respectively, which are defined using the rotational angle.

dx.doi.org/10.1021/ct500027z | J. Chem. Theory Comput. 2014, 10, 2005–2015

Table 3. Isotropic Hyperfine Coupling Constants (HFCCs) of Muon and Proton in Muoniated and Hydrogenated Ethyl Radicals by Several Methods and Experiments [in MHz]

	conventional[a]			quantum			exptl.	
HFCC	O3LYP[b]	O3LYP[c]	CCSD(T)[d]	Mu radical	H radical	classical	Mu radical[e]	H radical[f]
A_μ	(478.9)[g]	(493.8)[g]		372.6			329.8	
A'_μ	150.5	155.1	n/a	117.0			103.6	
A_{P_β}	36.9	38.0	n/a	66.8			66.8	
$\bar{A}_\beta$	74.7	77.0	65.0	83.6	77.6	73.7	79.1	75.3
A_{P_α}	−74.6	−63.8	−68.0	−70.8	−72.5	−71.9	−63.4	−62.7

[a]The static conventional methods cannot distinguish HFCCs in the Mu radical from those in the H radical. [b]The results of the static conventional O3LYP/6-31G(d,p) method at the EQ structure. [c]The results of the static conventional O3LYP functional with Chipman basis set at the EQ structure. [d]The CCSD(T)/TZ2P results were drawn from in Table 4 of ref 100. [e]All of HFCC values except for A_{P_α} were measured in the gas phase at 298.3 K; A_{P_α} was at 297.4 K (ref 70). [f]The measurement was done in liquid ethane at 93 K. According to ref 101, these are independent of temperature within experimental error. [g]The products of A'_μ by 3.183.

same plane in contrast to the previous work based on a *static* concept[99] and the large-amplitude rocking distribution becomes frequent when the rotational angle is close to 60°, 180°, and 300°. Particularly, for planarity involving the methylene group, quantum simulations predict rocking angles larger than those from static conventional calculations. This would be attributed to the internal rotation as was suggested in ref 62 and the Coulomb repulsion between an unpaired electron and electrons associated with the expanding nuclear clouds. In the Mu radical, the methylene-group inversion promotes the less stable configurations with the radical orbital oriented *syn* to the methyl C_β−Mu bond in Figure 5a. Meanwhile, in the H radical, as seen in Figure 5b, the inversion enhances localization of stable configurations and makes a difference in FEL in the large rocking angle. The nearly symmetric distribution indicates that the methylene-group inversion in the H radical takes place much more frequently than that in the Mu radical. The 2D FELs using the signed rocking angle suggest that at 300 K frequent inversion of the methylene group blurs the *pure* methyl-group rotation.

The methylene-group rocking motions enable the rotational barrier heights to be 0.29 and 0.72 kcal/mol for the H and Mu radicals, respectively (see text and Figure S3 in the Supporting Information). These theoretical values are closer to the experimentally estimated values (0.05 and 0.7 kcal/mol) compared to those in Figure 3. Thus, it can be stated that the *apparent* height as a result of the coupling between the motions, including the methyl-group rotation and methylene-group rocking motion, is monitored experimentally. There still remains some difference in barrier height in the H radical. This would be expected to result from the contribution of other motions such as the methyl-group umbrella and rocking motions to the rotation, because the methylene-group inversion occurs in various conformations in the H radical.

3.4. Quantum Simulation: Prediction of Isotropic Hyperfine Coupling Constants. Geometric configurations from our *ab initio* PIMD simulations yield isotropic HFCCs shown in Table 3. For comparison of these simulations, the conventional results of the O3LYP/6-31G(d,p), the O3LYP with Chipman basis set (O3LYP/Chipman), and the CCSD-(T)/TZ2P methods as well as the corresponding experimental values in the gas phase at about 300 K are also listed.[32,70,100,101] In the quantum columns, the averages of HFCC values obtained at each imaginary step over the PIMD production runs are given. Similarly, the classical term provides the average HFCC values over the sampling period. Note that in the conventional columns, HFCCs in the Mu radical are equal to those in the H one, because the mass of the nucleus does not affect an electronic structure within the static conventional approach. A_μ is the μ^+ HFCC, and A'_μ is the reduced μ^+ HFCC to facilitate the comparison with H^+ HFCC, expressed by

$$A'_\mu = \frac{\mu_p}{\mu_\mu} A_\mu \tag{11}$$

where μ_p and μ_μ are the magnetic moments of the proton and positive muon, respectively. A_{P_β} and A_{P_α} denote the average HFCC of the two β protons (H_2 and H_3 nuclei) and that of the α protons (H_4 and H_5 nuclei), respectively. $\bar{A}_\beta$ is the average of the HFCCs of the methyl protons; it is represented by

$$\bar{A}_\beta = \frac{(A'_\mu + 2A_{P_\beta})}{3} \tag{12}$$

for the Mu radical.

Table 3 reveals that our PIMD results in the methyl group are in remarkable agreement with the experimental results. Compared to the experimental results for the Mu radical, although the conventional A'_μ is overestimated by 45−50%, the PIMD result shows a 13.0% overestimation; A_{P_β} from the conventional method is underestimated by 43−45%, whereas in the PIMD result it is quite similar to the experimental value. The results of $\bar{A}_\beta$ for both radicals are close to the experimental ones, regardless of theoretical approaches. Strictly speaking, the PIMD result slightly overestimates the experimental value, whereas other results with the O3LYP/6-31G(d,p) method underestimate it. The PIMD simulation provides A_{P_α} in the Mu radical differing from that in the H radical, and the difference between these values is small, corresponding to the experimental result. In addition, because HFCC values in the H radical were measured in the liquid ethane, where solvent effects on this radical cause $\bar{A}_\beta$ and $|A_{P_\alpha}|$ to decrease from those in the gas phase to a small extent, it is difficult to compare the experimental trend in A_{P_α} between the radicals with the theoretical one. As a result, our PIMD results have a tendency to overestimate the experimental ones to a small extent.

Now, let us focus on the electronic structure calculation employed in this study. The O3LYP/6-31G(d,p) method is appropriate to describe the potential energy surface and structural fluctuations of both the radicals, as shown in subsections 3.1−3.3. However, Table 3 shows that this method

apparently is not enough for highly accurate HFCC calculation, especially for the HFCC value of the α proton, reflecting the spin polarization by the *intragroup* interaction. In particular, the 6-31G(d,p) basis set is not sufficiently flexible to describe the spin-polarized electronic structure of the methylene group in various geometric configurations. The value of the O3LYP/Chipman method is closer to the experimental value than that of the CCSD(T)/TZ2P method. The differences between PIMD and experimental values can be expected to be much smaller by employing the large tailored basis set. Hence, errors of the HFCC values do not result from the inefficiency of the sampling of both μ^+ and H^+ clouds and/or molecular structures of the Mu/H radicals, necessary to represent nuclear quantum and thermal effects.

As mentioned in subsection 3.3, the ratio of the C_β–Mu bond length to the EQ one is 1.057 in this study, somewhat larger than 1.049 that is the scale factor proposed by Roduner and Reid.[102] This suggests that it is difficult to determine the universal ratio for the bond length to represent the residual isotope effect. When the EQ structure of the Mu radical with this effect is defined as the structure optimized with one C_β–H bond length fixed to 1.158 Å, obtained with 1.049 × 1.104 Å ($R_{C_\beta Mu}$ of the above-mentioned EQ structure), the reduced HFCC A'_μ is calculated as 168.2 MHz. Although average $\bar{A}_\beta$ becomes better (80.4 MHz), A'_μ is far from the experimental value of 103.6 MHz in the gas phase at 300 K.[103] This suggests that the structural fluctuations due to both the nuclear quantum and thermal effects, not just the bond stretching motion, play a crucial role in theoretical prediction, giving μ^+ and H^+ HFCCs comparable to the experimental ones.

3.5. Quantum Simulation: Role of Geometric Structure in μ^+ and Methyl H^+ HFCC Values. Let us explain the influence of geometric structure on the difference in HFCC values between the Mu and H radicals. At first, to understand how μ^+ and methyl H^+ HFCCs are distributed, 1D FECs along A'_μ and $\bar{A}_\beta$ for the H radical are given in Figure 6. Figure 6

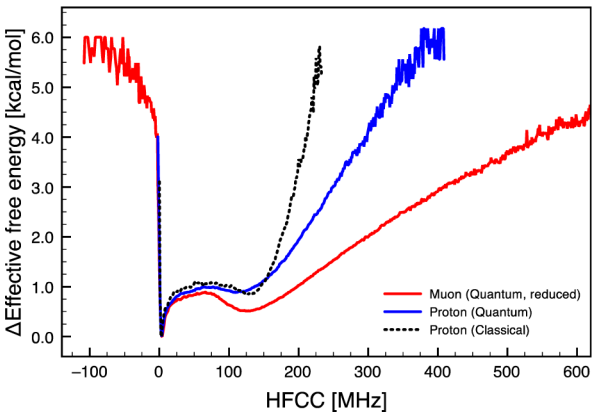

Figure 6. Effective free energy curves along isotropic reduced μ^+ HFCC (A'_μ) for muoniated ethyl radical and along isotropic methyl H^+ HFCC ($\bar{A}_\beta$) for hydrogenated ethyl radicals from nuclear quantum and classical simulations.

shows that both the HFCCs exhibit the first minimum around 5 MHz, while the second minimum of A'_μ around 130 MHz is much deeper than that of $\bar{A}_\beta$ for the H radical. It is plausible that the broader distribution of the Mu radical in the large HFCC region reflects the larger amplitude of the C_β–Mu stretching and expansion of the μ^+ cloud, compared to the H radical. Note that this distribution causes the narrow distribution around 5 MHz to appear to be the global minimum. In addition to such a broad distribution, the second minimum is of importance for the μ^+ HFCC value being large; it may be attributed to the residual isotope effect mentioned in subsection 3.3. Furthermore, Figure 6 reveals that unique structures, which yield large negative HFCC values, are found in only the Mu radical (see text and Figure S6 in the Supporting Information for further discussion).

Next, the origin of the characteristic second minimum of the A'_μ FEC (Figure 6) using two different 2D FELs is discussed. The 2D FELs as a function of A'_μ and $R_{C_\beta Mu}$ and of $\bar{A}_\beta$ for the H radical and $\bar{R}_{C_\beta H}$ are given in Figure 7a and b, respectively.

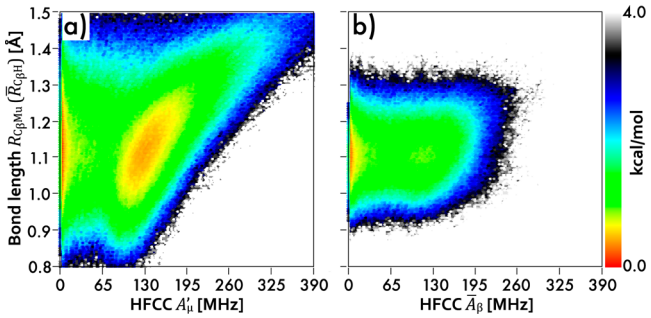

Figure 7. Free energy landscapes as a function (a) of the reduced μ^+ HFCC (A'_μ) and C_β–Mu bond length ($R_{C_\beta Mu}$) and (b) of the methyl H^+ HFCC ($\bar{A}_\beta$) and the C_β–H bond length averaged over the three equivalent bonds ($\bar{R}_{C_\beta H}$).

These FELs clearly show that there are uncorrelated and correlated regions of HFCC values with the bond length, and these two regions are distinguished by the HFCC value of about 70 MHz. The broad distribution in the large μ^+ HFCC region including the target minimum is found in the correlated region. In general, as seen in the discussion of the scale factor, the bond elongation causes the HFCC value to be large, because the spin polarization contributing significantly to HFCC is enhanced. However, in the other region, a bond length variation does not act on the HFCC values, always being small. This means that the radical orbital containing an unpaired electron has little influence on the C_β–Mu/H bond in the uncorrelated region because of their relative position (see Figure S5). Hence, the position of the C_β–Mu bond relative to the radical orbital produces the two regions, and its locality, as shown in Figures 4 and 5, leads to the second minimum of the A'_μ FEC.

From the discussion presented in this paper, we conclude the following. In the Mu radical, the rotational angle ($\phi_{MuC_\beta C_\alpha X}$) is usually at 0° or 180°. At $\phi_{MuC_\beta C_\alpha X}$ = 0°/180°, a large variation in the C_β–Mu bond length can cause a wide range of A'_μ. In the H radical, the methyl group is free to rotate at 300 K, while the rotational angle ($\phi_{HC_\beta C_\alpha X}$) is often at 60°, 180°, or 300°. At $\phi_{HC_\beta C_\alpha X}$ = 60°/180°/300°, a moderate variation in the C_β–H bond length can only give a small range of $\bar{A}_\beta$ for the H radical, which is hardly correlated with the bond length. The HFCC values, bond stretching motion in the methyl group, rotation of this group, and methylene-group rocking motion complexly intertwine with each other. Therefore, the unique second minimum in the A'_μ FEC is attributed to the specific behavior of the CH_2Mu group distinct from the CH_3 group, resulting

dx.doi.org/10.1021/ct500027z | J. Chem. Theory Comput. 2014, 10, 2005−2015

from molecular motions and their coupling. It can be stated that overall molecular motion rather than only the C_β–H stretching motion produces the residual isotope effect. The difference in molecular behavior, especially the methyl rotation, arising from the C_β–Mu bond elongation plays an essential role in the μ^+-HFCC prediction; in other words, geometric configurations reflecting the nuclear quantum and thermal effects enable us to accurately predict HFCC values in muoniated as well as hydrogenated radicals. We confirm that *ab initio* PIMD simulations facilitate the understanding of the nature of muoniated radicals.

4. CONCLUDING REMARKS

A quantitative evaluation of properties, which are dictated by an electron density at the nuclear position, is challenging because it is difficult to represent such density with well-used theoretical methods. The isotropic hyperfine coupling constant (HFCC), one of these properties, has been predicted using an *ab initio* path integral molecular dynamics (PIMD) simulation with density functional theory (DFT) potential. This simulation can consider nuclear quantum and thermal effects, which are not treated by static conventional theoretical methods. Because small mass makes the former effect larger, a bound state of positive muon with one-ninth of a proton mass and electron, i.e., muonium (Mu) was focused. We demonstrated the capability of *ab initio* PIMD simulation to be applied to a Mu-substituted (muoniated) ethyl radical ($C_\beta H_2Mu–C_\alpha H_2$) in addition to unsubstituted (hydrogenated) ethyl radicals ($C_\beta H_3–C_\alpha H_2$).

Conformational analyses with the static conventional O3LYP/6-31G(d,p) calculations show that the shape of the potential energy curve of the H radical along the rotational angle changes with the elongation of one methyl C_β–H bond, and then the bond length and rotational angle are interdependent. This is because the elongation shifts the balance of attractive and repulsive interactions between the methyl and methylene groups. The results of the PIMD simulations reveal that for both the radicals the average bond lengths are longer than equilibrium ones from the static conventional calculation. Because the bond elongation is proportional to the magnitude of the anharmonicity of the potential along bonds, the C_β–Mu bond is more elongated than the C_β–H bonds, thereby resulting in the unbalanced $C_\beta H_2Mu$ group. This group exhibits a rotational motion distinct from the $C_\beta H_3$-group rotation judging from the free energy curves (FECs) with respect to the rotational angle. The free energy landscapes (FELs) show that the C_β–Mu/H bond stretching is confined to the region depending on the rotational angle. The FELs involving the rocking angle reveal that the methylene-group rocking motions, including inversion, behave differently in the Mu and H radicals and have a significant influence on the methyl-group rotation.

For both the radicals, HFCC values in the methyl groups obtained from the PIMD simulations are in good accord with the corresponding experimental values. Meanwhile, using static conventional calculations with a scale factor, HFCC values for the bond-elongated ethyl radical are poorly estimated. The FELs involving HFCC demonstrate that HFCC values in the Mu and H radicals are essentially correlated and uncorrelated, respectively, with both the C_β–Mu/H bond and rotational angle. Thus, the C_β–Mu/H bond stretching motion, methyl-group rotation, methylene-group rocking motion, and HFCC values cannot be treated separately. The PIMD simulations with reliable potential successfully describe the intrinsic molecular motion of each radical, which is represented as various geometric configurations reflecting the nuclear quantum and thermal fluctuations. The proper consideration of such a motion is important for an accurate estimation of HFCC values. In particular, the unique $C_\beta H_2Mu$-group behavior is responsible for a fundamental difference in HFCC between muon and proton. Further, it is expected that much more computationally demanding PIMD simulation using a large tailored basis set for HFCC prediction will provide more accurate HFCC values. We can assert that from a theoretical perspective, the *ab initio* PIMD approach with reliable potential contributes to the development of muon and muonium chemistry.

■ ASSOCIATED CONTENT

Supporting Information

Details of the NBO analysis (subsection 3.2), the rotational barrier heights with the influence of the methylene-group rocking motion (subsection 3.3), and the unique structures (subsection 3.5) are provided, together with Figures S1–S8 and Chart S1. This material is available free of charge via the Internet at http://pubs.acs.org/.

■ AUTHOR INFORMATION

Corresponding Author

*E-mail: tachi@yokohama-cu.ac.jp.

Present Address

[§]Fukui Institute for Fundamental Chemistry, Kyoto University, Takano-Nishihiraki-cho 34–4, Sakyo-ku, Kyoto 606–8103, Japan

Notes

The authors declare no competing financial interest.

■ ACKNOWLEDGMENTS

Financial support was provided by Grant-in-Aid for Scientific Research and for the priority area by Ministry of Education, Culture, Sports, Science and Technology, Japan for Y.K. and M.T.

■ REFERENCES

(1) Percival, P. W. *Radiochim. Acta* **1979**, *26*, 1–14.
(2) Fleming, D. G.; Garner, D. M.; Vaz, L. C.; Walker, D. C.; Brewer, J. H.; Crowe, K. M. *Positronium and Muonium Chemistry. Advances in Chemical Series*; Ache, H. J., Ed.; American Chemical Society: Washington, DC, 1979; Vol *175*, pp 279–334.
(3) Walker, D. C. *Muon and Muonium Chemistry*; Cambridge University Press: Cambridge, U. K., 1983.
(4) Percival, P. W. *Hyperfine Interact.* **1990**, *65*, 901–911.
(5) Claxton, T. A. *Chem. Soc. Rev.* **1995**, *24*, 437–448.
(6) Rhodes, C. J. *J. Chem. Soc., Perkin Trans. 2* **2002**, 1379–1396.
(7) McKenzie, I.; Roduner, E. *Naturwissenschaften* **2009**, *96*, 873–87.
(8) Roduner, E.; Fischer, H. *Chem. Phys.* **1981**, *54*, 261–276.
(9) Symons, M. C. R. *Hyperfine Interact.* **1984**, *19*, 771–783.
(10) McKenzie, I. *Annu. Rep. Prog. Chem., Sect. C: Phys. Chem.* **2013**, *109*, 65–112.
(11) Walker, D. C. *J. Chem. Soc., Faraday Trans.* **1998**, *94*, 1–9.
(12) Cohen, J. *Phys. Rev. A* **1999**, *59*, 1160–1169.
(13) Jones, S. E.; Anderson, A. N.; Caffrey, A. J.; Walter, J. B.; Watts, K. D.; Bradbury, J. N.; Gram, P. A. M.; Leon, M.; Maltrud, H. R.; Paciotti, M. A. *Phys. Rev. Lett.* **1983**, *51*, 1757–1760.
(14) Jones, S. E. *Nature* **1986**, *321*, 127–133.
(15) Breunlich, W. H.; Kammel, P.; Cohen, J. S.; Leon, M. *Annu. Rev. Nucl. Part. Sci.* **1989**, *11*, 255–264.

(16) Clary, D. C.; Connor, J. N. L. *J. Phys. Chem.* **1984**, *88*, 2758−2764.
(17) Ghandi, K.; Cottrell, S. P.; Fleming, D.; Johnson, C. *Phys. B* **2006**, *374*−*375*, 303−306.
(18) Fleming, D. G.; Cottrell, S. P.; McKenzie, I.; Macrae, R. M. *Phys. Chem. Chem. Phys.* **2012**, *14*, 10953−10966.
(19) Lappas, A.; Prassides, K.; Vavekis, K.; Arcon, D.; Blinc, R.; Cevc, P.; Amato, A.; Feyerherm, R.; Gygax, F. N.; Schenck, A. *Science* **1995**, *267*, 1799−1802.
(20) Amato, A. *Rev. Mod. Phys.* **1997**, *69*, 1119−1179.
(21) Storchak, V.; Brewer, J.; Morris, G.; Arseneau, D.; Senba, M. *Phys. Rev. B* **1999**, *59*, 10559−10572.
(22) Bewley, R. I.; Blundell, S. J.; Lovett, B. W.; Jestädt, T.; Pratt, F. L.; Chow, K. H.; Hayes, W.; Battle, P. D.; Green, M. A.; Millburn, J. E.; Rosseinsky, M. J.; Spring, L. E.; Vente, J. F. *Phys. Rev. A* **1999**, *60*, 286−293.
(23) Dunsiger, S.; Gardner, J.; Chakhalian, J.; Cornelius, A.; Jaime, M.; Kiefl, R.; Movshovich, R.; MacFarlane, W.; Miller, R.; Sonier, J.; Gaulin, B. *Phys. Rev. Lett.* **2000**, *85*, 3504−3507.
(24) Gatteschi, D.; Carretta, P.; Lascialfari, A. *Physica A* **2000**, *290*, 94−105.
(25) Chow, K. H.; Kiefl, R. F.; Hitti, B.; Estle, T. L.; Lichti, R. L. *Phys. Rev. Lett.* **2000**, *84*, 2251−2254.
(26) Cammarere, D.; Scheicher, R. H.; Sahoo, N.; Das, T. P.; Nagamine, K. *Phys. B* **2000**, *289*−*290*, 636−639.
(27) Lossack, A. M.; Roduner, E.; Bartels, D. M. *Phys. Chem. Chem. Phys.* **2001**, *3*, 2031−2037.
(28) Frosch, R. A.; Foley, H. M. *Phys. Rev.* **1952**, *88*, 1337−1349.
(29) Feller, D.; Davidson, E. R. *Theor. Chim. Acta* **1985**, *68*, 57−67.
(30) Chipman, D. M. *Quantum Mechanical Electronic Structure Calculations with Chemical Accuracy*; Langhoff, S. R., Ed.; Kluwer Academic Publishers: Dordrecht, The Netherlands, 1995; p 109.
(31) Engels, B.; Eriksson, L. A. *Advances in Quantum Chemistry*; Löwdin, P.-O., Sabin, J. R., Zerner, M. C., Eds.; Academic Press: San Diego, CA, 1996; p 297.
(32) Chipman, D. M. *Theor. Chim. Acta* **1989**, *76*, 73−84.
(33) Chipman, D. M. *Theor. Chim. Acta* **1992**, *82*, 93−115.
(34) Perera, S. A.; Watts, J. D.; Bartlett, R. J. *J. Chem. Phys.* **1994**, *100*, 1425−1434.
(35) Improta, R.; Barone, V. *Chem. Rev.* **2004**, *104*, 1231−54.
(36) Donovan, E.; Kongsted, J.; Sauer, S. P. A. *J. Chem. Theory Comput.* **2011**, *7*, 4077−4087.
(37) Hedega, E. D.; Kongsted, J.; Sauer, S. P. A. *J. Chem. Theory Comput.* **2013**, *9*, 2380−2388.
(38) Pan, X.; Sahni, V. *Phys. Rev. A* **2003**, *67*, 012501−1−012501−5.
(39) Perdew, J. P.; Ruzsinszky, A.; Tao, J.; Staroverov, V. N.; Scuseria, G. E.; Csonka, G. I. *J. Chem. Phys.* **2005**, *123*, 062201−1−062201−9.
(40) Eriksson, L. A.; Malkin, V. G.; Malkina, O. L.; Salahub, D. R. *J. Chem. Phys.* **1993**, *99*, 9756−9763.
(41) Eriksson, L. A.; Wang, J.; Boyd, R. J.; Lunell, S. *J. Phys. Chem.* **1994**, *98*, 792−799.
(42) Barone, V. *Recent Advances in Density Functional Methods, Part I*; Chong, D. P., Ed.; World Scientific Publ. Co.: Singapore, 1996.
(43) Hermosilla, L.; Calle, P.; García de la Vega, J. M.; Sieiro, C. *J. Phys. Chem. A* **2005**, *109*, 1114−1124.
(44) McCollum, B. M.; Abe, T.; Brodovitch, J.-C.; Clyburne, J. a C.; Iwamoto, T.; Kira, M.; Percival, P. W.; West, R. *Angew. Chem., Int. Ed.* **2008**, *47*, 9772−9774.
(45) West, R.; Percival, P. W. *Daltron Trans.* **2010**, *39*, 9209−9216.
(46) Percival, P. W.; Brodovitch, J.-C.; Mozafari, M.; Mitra, A.; West, R.; Ghadwal, R. S.; Azhakar, R.; Roesky, H. W. *Chem.−Eur. J.* **2011**, *17*, 11970−11973.
(47) Percival, P. W.; Ramos, M.; Webster, B. C. *Chem. Phys.* **1982**, *67*, 275−285.
(48) Yu, D.; Percival, P. W.; Brodovitch, J.; Leung, S.; Kiefl, R. F.; Venkateswaran, K.; Cox, S. F. J. *Chem. Phys.* **1990**, *142*, 229−236.
(49) Chen, Y. K.; Fleming, D. G.; Wang, Y. A. *J. Phys. Chem. A* **2011**, *115*, 2765−2777.
(50) Tuckerman, M. E.; Marx, D.; Klein, M. L.; Parrinello, M. *Science* **1997**, *275*, 817−820.
(51) Ishimoto, T.; Tachikawa, M.; Nagashima, U. *Int. J. Quantum Chem.* **2009**, *109*, 2677−2694.
(52) Tachikawa, M.; Shiga, M. *J. Am. Chem. Soc.* **2005**, *127*, 11908−11909.
(53) Kawashima, Y.; Tachikawa, M. *Chem. Phys. Lett.* **2013**, *571*, 23−27.
(54) Shiga, M.; Tachikawa, M.; Miura, S. *Chem. Phys. Lett.* **2000**, *332*, 396−402.
(55) Shiga, M.; Tachikawa, M.; Miura, S. *J. Chem. Phys.* **2001**, *115*, 9149−9159.
(56) Garrett, B. C.; Truhlar, D. G.; Melius, C. F. *Phys. Rev. A* **1981**, *24*, 2853−2856.
(57) Böhm, M. C.; Ramírez, R.; Schulte, J. *Mol. Phys.* **2005**, *103*, 2407−2436.
(58) Chipman, D. M. *J. Chem. Phys.* **1991**, *94*, 6632−6637.
(59) Pacansky, J.; Dupuis, M. *J. Chem. Phys.* **1978**, *68*, 4276−4278.
(60) Carmicbael, I. *J. Phys. Chem.* **1991**, *95*, 6198−6201.
(61) Suter, H. U.; Ha, T.-K. *Chem. Phys.* **1991**, *154*, 227−236.
(62) Sears, T. J.; Johnson, P. M.; Jin, P.; Oatis, S. *J. Chem. Phys.* **1996**, *104*, 781−792.
(63) East, A. L. L.; Bunker, P. R. *Chem. Phys. Lett.* **1998**, *282*, 49−53.
(64) Sears, T. J.; Johnson, P. M.; BeeBe-Wang, J. *J. Chem. Phys.* **1999**, *111*, 9213−9221.
(65) Johnson, P. M.; Sears, T. J. *J. Chem. Phys.* **1999**, *111*, 9222−9226.
(66) Schulte, J.; Böhm, M. C.; Ramírez, R.; López-Ciudad, T. *Mol. Phys.* **2005**, *103*, 105−127.
(67) Bridges, M. D.; Arseneau, D. J.; Fleming, D. G.; Ghandi, K. *J. Phys. Chem. C* **2007**, *111*, 9779−9793.
(68) Ramos, M. J.; McKenna, D.; Webster, B. C.; Roduner, E. *J. Chem. Soc. Faraday, Trans. 1* **1984**, *80*, 255−265.
(69) Roduner, E.; Garner, D. M. *Hyperfine Interact.* **1986**, *32*, 733−739.
(70) Percival, P. W.; Brodovitch, J.-C.; Leung, S.-K.; Yu, D.; Kiefl, R. F.; Garner, D. M.; Arseneau, D. J.; Fleming, D. G.; Gonzalez, A.; Kemptqn, J. R.; Senba, M.; Venkateswaran, K.; Cox, S. F. J. *Chem. Phys. Lett.* **1989**, *163*, 241−245.
(71) Claxton, T. A.; Graham, A. M. *J. Chem. Soc., Faraday Trans. 2* **1987**, *83*, 2307−2317.
(72) Webster, B. C.; Macrae, R. *Chem. Phys. Lett.* **1988**, *150*, 18−22.
(73) Webster, B.; Buttart, D. *J. Chem. Soc., Faraday Trans.* **1996**, *92*, 2331−2334.
(74) Cox, S. F. J.; Claxton, T. A.; Symons, M. C. R. *Int. J. Radiat. Appl. Instrum., Part C: Radiat. Phys. Chem.* **1986**, *28*, 107−113.
(75) Yamada, K.; Kawashima, Y.; Tachikawa, M. *Chin. J. Phys.* **2013**, Accepted.
(76) Tachikawa, M.; Shiga, M. *J. Chem. Phys.* **2004**, *121*, 5985−5991.
(77) Berne, B. J.; Thirumalai, D. *Annu. Rev. Phys. Chem.* **1986**, *37*, 401−424.
(78) Marx, D.; Parrinello, M. *Z. Phys. B: Condens. Matter* **1994**, *95*, 143−144.
(79) Martyna, G. J.; Klein, M. L.; Tuckerman, M. *J. Chem. Phys.* **1992**, *97*, 2635−2643.
(80) Frisch, M. J.; Trucks, G. W.; Schlegel, H. B.; Scuseria, G. E.; Robb, M. A.; Cheeseman, J. R.; Scalmani, G.; Barone, V.; Mennucci, B.; Petersson, G. A.; Nakatsuji, H.; Caricato, M.; Li, X.; Hratchian, H. P.; Izmaylov, A. F.; Bloino, J.; Zheng, G.; Sonnenberg, J. L.; Hada, M.; Ehara, M.; Toyota, K.; Fukuda, R.; Hasegawa, J.; Ishida, M.; Nakajima, T.; Honda, Y.; Kitao, O.; Nakai, H.; Vreven, T.; Montgomery, J. A., Jr.; Peralta, J. E.; Ogliaro, F.; Bearpark, M.; Heyd, J. J.; Brothers, E.; Kudin, K. N.; Staroverov, V. N.; Kobayashi, R.; Normand, J.; Raghavachari, K.; Rendell, A.; Burant, J. C.; Iyengar, S. S.; Tomasi, J.; Cossi, M.; Rega, N.; Millam, J. M.; Klene, M.; Knox, J. E.; Cross, J. B.; Bakken, V.; Adamo, C.; Jaramillo, J.; Gomperts, R.; Stratmann, R. E.; Yazyev, O.; Austin, A. J.; Cammi, R.; Pomelli, C.; Ochterski, J. W.; Martin, R. L.; Morokuma, K.; Zakrzewski, V. G.; Voth, G. A.; Salvador, P.; Dannenberg, J. J.; Dapprich, S.; Daniels, A. D.; Farkas, Ö.;

Foresman, J. B.; Ortiz, J. V.; Cioslowski, J.; Fox, D. J. *Gaussian 09*, rev C.01; Gaussian, Inc.: Wallingford, CT, 2009.
(81) Purvis, G. D., III; Bartlett, R. J. *J. Chem. Phys.* **1982**, *76*, 1910−1918.
(82) Head-Gordon, M.; Pople, J. A.; Frisch, M. J. *Chem. Phys. Lett.* **1988**, *153*, 503−506.
(83) Dunning, T. H., Jr. *J. Chem. Phys.* **1989**, *90*, 1007−1023.
(84) Perdew, J. P. *Phys. Rev. B* **1986**, *33*, 8822−8824.
(85) Lee, C.; Yang, W.; Parr, R. G. *Phys. Rev. B* **1988**, *37*, 785−789.
(86) Becke, A. D. *J. Chem. Phys.* **1993**, *98*, 5648−5652.
(87) Burke, K.; Perdew, J. P.; Wang, Y. *Electronic Density Functional Theory: Recent Progress and New Directions*; Dobson, J. F., Vignale, G., Das, M. P., Eds.; Plenum: New York, 1998; pp 81−111.
(88) Cohen, A. J.; Handy, N. C. *Mol. Phys.* **2001**, *99*, 607−615.
(89) Zhao, Y.; Truhlar, D. G. *Theor. Chem. Acc.* **2007**, *120*, 215−241.
(90) Chai, J.-D.; Head-Gordon, M. *J. Chem. Phys.* **2008**, *128*, 084106−1−084106−15.
(91) Hehre, W. J.; Ditchfield, R.; Pople, J. A. *J. Chem. Phys.* **1972**, *56*, 2257−2261.
(92) Hariharan, P. C.; Pople, J. A. *Theor. Chim. Acta* **1973**, *28*, 213−222.
(93) Foster, J. P.; Weinhold, F. *J. Am. Chem. Soc.* **1980**, *4*, 7211−7218.
(94) Reed, A. E.; Curtiss, L. A.; Weinhold, F. *Chem. Rev.* **1988**, *88*, 899−926.
(95) Roduner, E.; Stolma, M.; Dilger, H.; Reid, I. D. *J. Phys. Chem. A* **1998**, *102*, 7591−7597.
(96) Clough, S.; Poldy, F. *J. Chem. Phys.* **1969**, *51*, 2076−2084.
(97) Toriyama, K.; Iwasaki, M.; Nunome, K.; Muto, H. *J. Chem. Phys.* **1981**, *75*, 1633−1638.
(98) Ramos, M. J.; McKenna, D.; Webster, B. C.; Roduner, E. *J. Chem. Soc., Faraday Trans. 1* **1984**, *80*, 267−274.
(99) Symons, M. C. R. *Struct. Chem.* **1991**, *2*, (225)433−(231)439.
(100) Perera, S. A.; Salemi, L. M.; Bartlett, R. J. *J. Chem. Phys.* **1997**, *106*, 4061−4066.
(101) Fessenden, R. W.; Schuler, R. H. *J. Chem. Phys.* **1963**, *39*, 2147−2195.
(102) Roduner, E.; Reid, I. E. *Isr. J. Chem.* **1989**, *29*, 3−11.
(103) The reduced HFCC with scale factor would become close to that experimentally observed at lower temperatures.